Neuron, Vol. 38, 187–199, April 24, 2003, Copyright ©2003 by Cell Press

Axon Regeneration in Young Adult Mice Lacking Nogo-A/B

Ji-Eun Kim,[1] Shuxin Li,[1] Tadzia GrandPré, Dike Qiu, and Stephen M. Strittmatter*
Department of Neurology
Department of Neurobiology
Yale University School of Medicine
New Haven, Connecticut 06510

Summary

After injury, axons of the adult mammalian brain and spinal cord exhibit little regeneration. It has been suggested that axon growth inhibitors, such as myelin-derived Nogo, prevent CNS axon repair. To investigate this hypothesis, we analyzed mice with a *nogo* mutation that eliminates Nogo-A/B expression. These mice are viable and exhibit normal locomotion. Corticospinal tract tracing reveals no abnormality in uninjured *nogo-A/B*$^{-/-}$ mice. After spinal cord injury, corticospinal axons of young adult *nogo-A/B*$^{-/-}$ mice sprout extensively rostral to a transection. Numerous fibers regenerate into distal cord segments of *nogo-A/B*$^{-/-}$ mice. Recovery of locomotor function is improved in these mice. Thus, Nogo-A plays a role in restricting axonal sprouting in the young adult CNS after injury.

Introduction

Axotomized peripheral axons exhibit a robust regenerative reaction after axotomy. In stark contrast, severed brain and spinal axons do not advance through the adult CNS. Instead, these fibers are trapped at the site of damage and remain disconnected from synaptic targets, leading to profound and persistent deficits in many clinical cases. Spinal cord injury (SCI) is the clearest example of a condition in which axonal disconnection leads to significant disability despite minimal neuronal death.

In part, the CNS/PNS axonal regenerative disparity can be explained by the selective capacity of peripheral neurons to express a gene repertoire after axotomy that promotes growth (Skene, 1989; Neumann and Woolf, 1999; Bonilla et al., 2002). However, several lines of evidence have suggested that the explanation for poor CNS axon regeneration is not cell autonomous. In particular, the studies of Aguayo and colleagues demonstrate long-distance growth of adult CNS axons in an appropriate environment, such as a sciatic nerve transplant (David and Aguayo, 1981; Benfey and Aguayo, 1982). Inhibitors of axon growth have been identified in the injured CNS. Astroglial scars at sites of damage produce chondroitin sulfate proteoglycans and inhibit axonal growth locally (Davies et al., 1999; Fawcett and Asher, 1999). Indeed, recent data indicate that digestion of chondroitin sulfates can lead to axonal sprouting and growth in the brain and spinal cord (Bradbury et al., 2002).

Most prominently, axon growth inhibitors have been identified in CNS myelin. Experimentally induced absence of myelin promotes axon regeneration (Savio and Schwab, 1990), and myelin-forming oligodendrocytes inhibit axon growth in vitro (Bandtlow et al., 1990). Myelin-associated glycoprotein (MAG) is one protein that inhibits axon outgrowth in vitro (Mukhopadhyay et al., 1994; McKerracher et al., 1994). In vivo, MAG has been shown to limit axon regeneration under certain conditions (Schäfer et al., 1996), although regeneration generally remains poor in the absence of MAG (Bartsch et al., 1995). The physiologic function of MAG appears not to be the limitation of axon growth, but rather participation in myelin stability by axoglial contact. Mice lacking MAG have delayed myelination, myelin splitting and redundancy, and decreased thickness of the periaxonal cytoplasmic collar of oligodendrocytes (Li et al., 1994; Montag et al., 1994). Over time, these myelin changes are associated with axonal degeneration (Fruttiger et al., 1995).

Another myelin-derived axon growth inhibitor is Nogo or Reticulon 4 (reviewed by GrandPré and Strittmatter, 2001). Analysis of the *nogo* expression reveals three mRNA species derived from two promotors and alternative splicing (GrandPré et al., 2000; Chen et al., 2000; Prinjha et al. 2000). Nogo-A is the major protein species in oligodendrocytes, with little or no Nogo-C in these cells and myelin (GrandPré and Strittmatter, 2001; Wang et al., 2002a; Huber et al., 2002). Both Nogo-C and Nogo-A are also found in neurons, while skeletal muscle produces Nogo-A embryonically and Nogo-C in the adult. Nogo-B is a minor form in brain. A 66 aa domain common to all Nogo forms is expressed on the surface of oligodendrocytes (GrandPré et al., 2000) and can potently inhibit axonal outgrowth by binding to an axonal Nogo-66 receptor (NgR; Fournier et al., 2001). A second amino-terminal domain of Nogo-A may also contribute to axon outgrowth inhibition by an undefined mechanism (Fournier et al., 2001). There appears to be a confluence of myelin inhibitory effects at the axonal NgR. Our investigations of NgR signaling mechanisms led to the realization that the NgR is a functional receptor for MAG as well as for Nogo-66 (Liu et al., 2002). Oligodendrocyte myelin glycoprotein (OMgp), a third CNS myelin-derived axon growth inhibitor, also acts through the NgR (Wang et al., 2002b).

The in vitro activity of Nogo-66 and the selective expression of Nogo in CNS but not PNS myelin are consistent with a role as a myelin-derived inhibitor of axonal regeneration after injury (GrandPré et al., 2000). In support of this hypothesis, the IN-1 antibody, recognizing Nogo and several other antigens, can promote CNS axon sprouting after injury (Bregman et al., 1995; reviewed by Bandtlow and Schwab, 2000). Similarly, but more selectively, a fragment of Nogo-66 with NgR antagonist properties enhances axonal regeneration after SCI (GrandPré et al., 2002). However, a role for Nogo in limiting CNS axonal regeneration has not been examined

*Correspondence: stephen.strittmatter@yale.edu
[1]These authors contributed equally to this work.

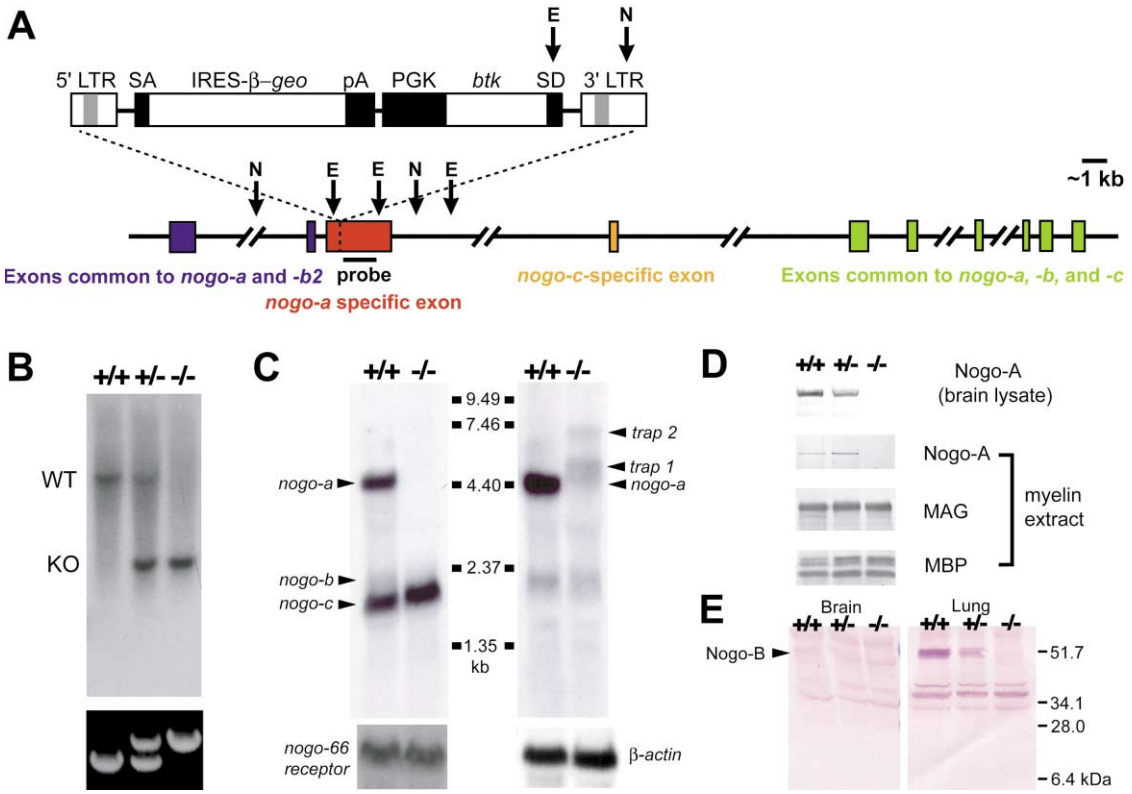

Figure 1. Disruption of the Mouse *nogo* Locus by Retroviral Gene-Trapping

(A) Diagram of the retroviral insertion. A restriction map illustrates the native exons of the mouse *nogo* gene and insertion of the 8.0 kb retroviral vector VICTR37 (not shown to scale) into the longest exon specific for Nogo-A.

(B) Southern blot and PCR analyses of Nhe I-digested genomic DNA from *nogo-A/B*$^{+/+}$, *nogo-A/B*$^{+/-}$, and *nogo-A/B*$^{-/-}$ mice. Hybridization with a PCR-amplified probe fragment (shown in A) yields an ~8–9 kb wild-type band and a shorter ~3 kb fragment from the disrupted gene. The bottom panel illustrates agarose gel separation of typical PCR reaction products from mouse genotyping.

(C) Northern blot analysis for *nogo*, *ngr*, and β-actin mRNA in the brains of *nogo-A/B*$^{+/+}$ and *nogo-A/B*$^{-/-}$ mice. The top left panel is from hybridization with a 3′ *nogo* probe detecting *nogo-A, -B*, and *-C,* as indicated. The top right panel is from hybridization with a 5′ *nogo-A* probe. The low-level expression of two novel transcripts from the mutated locus is demonstrated (*trap 1, trap 2*). Size markers are shown between the two panels.

(D) Immunoblot analysis for Nogo-A protein expression in total brain lysate and purified myelin extract from the brains of *nogo-A/B*$^{+/+}$, *nogo-A/B*$^{+/-}$, and *nogo-A/B*$^{-/-}$ mice. Myelin-associated glycoprotein (MAG) and myelin basic protein (MBP) were used as control myelin proteins.

(E) Anti-Nogo-A/B immunoblot in brain and lung lysates from *nogo-A/B*$^{+/+}$, *nogo-A/B*$^{+/-}$, and *nogo-A/B*$^{-/-}$ mice. Note the clear Nogo-B band in wild-type lung that is absent from the homozygous mutant mouse sample. No novel protein species of lesser molecular size containing the Nogo-A/B amino terminus are detected in the *nogo-A/B*$^{-/-}$ samples. Molecular size markers are shown at right.

with genetic methods. Here, we have analyzed mice lacking Nogo-A protein. The analysis reveals a role for Nogo-A in limiting axonal growth after axotomy in the adult CNS.

Results

Mice Lacking Nogo-A/B Are Viable

Embryonic stem cell lines in which the *nogo* gene had been "trapped" were identified from sequences of the trapped exons (Zambrowicz et al., 1998). A mouse strain established from these cells by blastocyst injection is viable in the homozygous state and selectively disrupts *nogo-A* and *nogo-B* expression. The gene trap insertion site maps near the 5′ end of the largest *nogo-A*-selective exon (Figures 1A and 1B). Based on the gene trap design and the insertion site, it is predicted that both *nogo-A* and *nogo-B*, but not *nogo-C,* expression will be disrupted by this insertion. Disrupted *nogo-A* and *nogo-B* transcripts are expected to contain the βgeo sequence and to be slightly larger than endogenous *nogo-A* mRNA, but they should lack sequences from the 3′ end of *nogo* that are common to all splice forms. Northern analysis with a probe from the 3′ common *nogo* region demonstrates a complete absence of *nogo-A* mRNA in the adult brain of homozygous *nogo-A/B*$^{-/-}$ mice (Figure 1C). The mRNA level for *nogo-B* in the adult brain of wild-type mice is quite low, and it is absent from the *nogo-A/B*$^{-/-}$ mice. The *nogo-C* and *ngr* expression levels are unchanged in this *nogo* gene trap line. A probe derived from the 5′ end of *nogo* corresponding to aa 30–145 encoded in exon 1 also demonstrates the absence of wild-type *nogo-A* transcripts in the *nogo-A/B*$^{-/-}$ brain. This 5′ *nogo-A* probe detects a relatively low level of at least two larger mRNA species that are consistent with βgeo fusion species derived from normal *nogo-A* splicing and from splicing of exon1 to the strong splice acceptor of the inserted DNA. Both forms are

expected to terminate at the polyadenylation sequence of the insert. The relatively reduced level of these novel mutated mRNA species is consistent with the insertion reducing either *nogo* transciption or *nogo*-β*geo* fusion mRNA stability.

Nogo-A protein of 205 kDa can be detected in the adult brain and in myelin preparations of wild-type mice with an antibody directed against a peptide encoded by a *nogo-A*-specific sequence 3′ to the location of the gene trap insertion site. Nogo-A is absent from the *nogo-A/B*$^{-/-}$ brain (Figure 1D). A second antiserum directed against the most amino-terminal region of Nogo-A and -B fails to detect significant levels of Nogo-B in the brain, but does demonstrate the presence of 51 kDa Nogo-B in wild-type lung tissue by immunoblot. In the *nogo-A/B*$^{-/-}$ lung, Nogo-B is absent (Figure 1E). The mutated *nogo*-β*geo* hybrid RNA has the potential to encode a truncated Nogo-A terminating at aa 309 and lacking both the Nogo-66 and the Amino-Nogo inhibitory domains. Contingent on the stability of the hydrophilic truncated Nogo-A 1–309 fragment, it might be produced as a soluble cytoplasmic protein. The strong splice acceptor of the construct is expected to trap erstwhile *nogo-B* transcripts so that a 1–168 aa protein might be formed in Nogo-B-producing cells. However, immunoblots of brain and lung with an amino-terminal directed anti-Nogo-A/B antibody fail to demonstrate any significant level of a novel smaller protein species (Figure 1E). This is likely due to reduced levels of the *nogo*-β*geo* hybrid mRNA as compared to wild-type *nogo-A* and due to the truncated protein instability. We conclude that this mutation in *nogo* effectively eliminates the expression of both Nogo-A and Nogo-B, but not Nogo-C.

On a mixed 129/C57Bl6J background, mice of the *nogo-A/B*$^{-/-}$ genotype are born at expected Mendelian frequencies and grow with normal body weights. Both males and females are fertile. No unexpected deaths have been witnessed in homozygous animals up to 12 months of age.

Normal Brain Histology and Behavior in Nogo-A Null Mice

Nogo-A, but not NgR, is distributed in many cell types of the developing CNS prior to oligodendrocyte maturation (Wang et al., 2002a). Therefore, Nogo-A could conceivably play a critical role in CNS patterning independent of NgR and myelin/axon interactions (Wang et al., 2002a; Huber et al., 2002). However, brain size and gross anatomy are normal in adult *nogo-A/B*$^{-/-}$ mice; there is no widespread failure of early developmental events. Major brain nuclei and the neuronal layers of the cerebral cortex and cerebellum are indistinguishable from those of wild-type mice by hematoxylin and eosin staining (Figures 2A, 2B, 2D, and 2E). Because the *nogo* gene insertion places *lacZ* under the control of the *nogo-A* regulatory elements (Figure 1A), those cells that would normally express Nogo-A can be identified by staining for β-galactosidase activity. In the cerebral cortex, the number and position of β-galactosidase-positive cells (Figure 2C) is very similar to Nogo-A-positive cells in wild-type mice (GrandPré et al., 2000; Wang et al., 2002a). The data indicate that neuronal placement and survival is normal in adult *nogo-A/B*$^{-/-}$ mice.

Of course, Nogo-A expression and function in oligodendrocytes is of the greatest interest. Luxol fast blue stains for total myelin content and location demonstrate normal patterns in young adult mice lacking Nogo-A (Figures 2G and 2H). Biochemically, myelin can be prepared from density gradient centrifugation in equal yield from wild-type, *nogo-A/B*$^{+/-}$, and *nogo-A/B*$^{-/-}$ mice (data not shown). Furthermore, such myelin preparations from mice of different genotype contain equal levels of MAG and myelin basic protein (Figure 1D). β-galactosidase-positive cells are visualized in the corpus callosum and deep cerebellar white matter with a location and distribution consistent with oligodendrocytes (Figures 2F and 2I). Qualitatively, the density and position of these β-galactosidase-positive cells is similar to that of CNPase-positive oligodendrocytes in wild-type mice. Thus, oligodendrocyte formation and survival appears normal in the absence of Nogo-A. The β-galactosidase expression demonstrates that the mutant chimeric *nogo*-β*geo* mRNA is stable enough to produce some detectable β-galactosidase protein within oligodendrocytes.

Despite the normal appearance of these histologic parameters, the absence of Nogo-A might change neuronal function and mouse behavior through effects on axonal performance. Qualitative neurological examination of the mice lacking Nogo-A reveals no deficits in function. Open-field behavioral parameters were not significantly different from littermate control mice (Figure 2J). There was a slight, but nonsignificant, trend toward decreased time in the center of an open field for the *nogo-A/B*$^{-/-}$ mice, a characteristic taken to correlate with measures of increased anxiety in other rodent experiments. The rotarod test assesses motor coordination and learning. No differences between mice with and without Nogo-A are observed on this test (Figure 2K). The BBB score is another measure of locomotor function in the open field and is commonly used to assess deficits after SCI (Basso et al., 1996). The uninjured *nogo-A/B*$^{-/-}$ mice exhibited a full range score of 21, similar to controls (data not shown). Overall, routine anatomical and locomotor analysis demonstrates no deficits in the *nogo-A/B* null mice.

CNS Myelin Lacking Nogo-A/B Does Not Inhibit Axonal Outgrowth

It is known that CNS myelin and Nogo-A can inhibit axonal growth in vitro. To determine whether Nogo-A is responsible for a significant fraction of myelin-dependent inhibition, we examined wild-type axons in the presence of myelin prepared from wild-type or *nogo-A/B*$^{+/-}$ or *nogo-A/B*$^{-/-}$ mice (Figure 3). All three preparations contain equal concentrations of MAG and MBP, differing only in Nogo-A concentration (Figure 1D). Wild-type or *nogo-A/B*$^{+/-}$ myelin potently collapses DRG growth cones, but *nogo-A/B*$^{-/-}$ myelin is 10 to 100 times less potent in this assay as a collapsing agent (Figures 4A and 4B). Chronic exposure to a substratum coated with wild-type CNS myelin inhibits neurite outgrowth. Eight-fold higher concentrations of myelin lacking Nogo-A are required to achieve the same level of inhibition (Figures 3A and 3C). This effect is more dramatic than that of the NEP1-40 peptide, which selectively

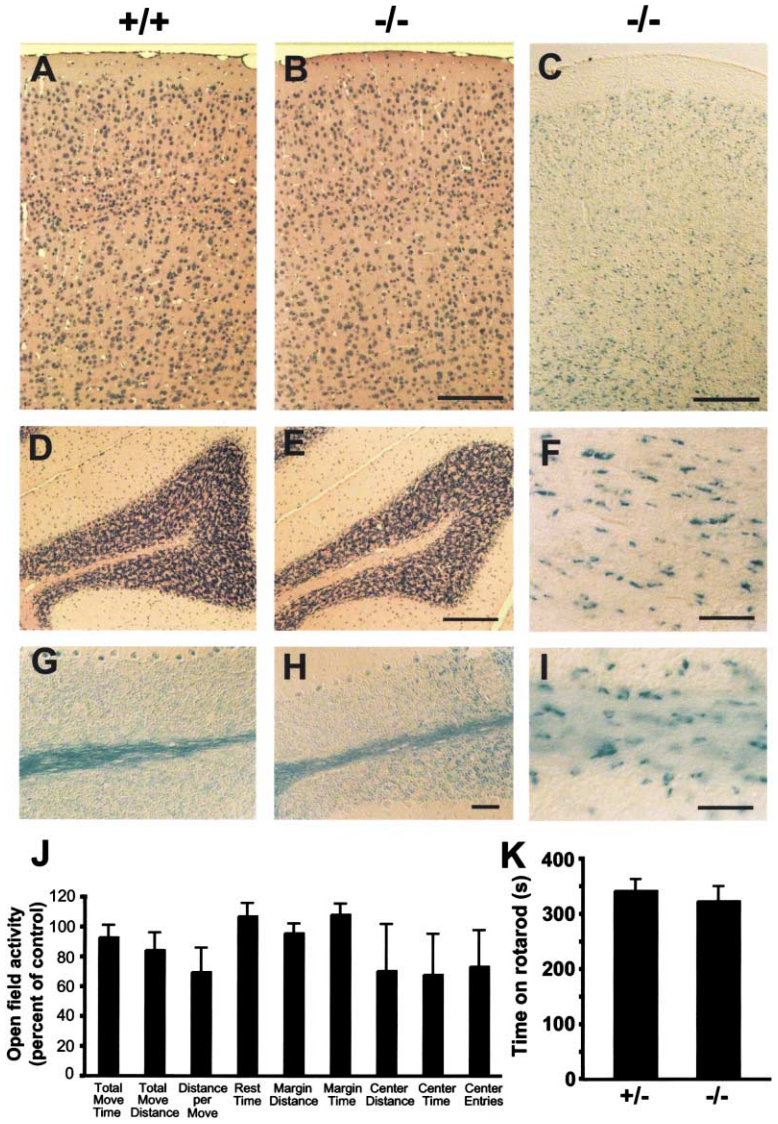

Figure 2. General Brain Histology and Locomotor Activity in *nogo-A/B*$^{-/-}$ Mice

(A–C) Coronal sections through the cerebral cortex stained with hematoxylin and eosin (A and B) or X-gal (C).

(D, E, and G–I) Parasagittal sections through the cerebellum stained with hematoxylin and eosin (D and E), Luxol fast blue (G and H), or X-gal (I).

(F) Corpus callosum in coronal sections stained with X-gal.

Scale bars equal 200 μm (A–E) and 50 μm (F–I).

(J) Open-field activity. Floor plane sensor measurements collected from an automated activity monitoring cage for *nogo-A/B*$^{-/-}$ mice shown as a percent of *nogo-A/B*$^{+/-}$ mice.

(K) Rotarod test. The time that mice were able to remain on the rotating rod at constantly accelerating speeds is reported.

blocks Nogo-66 action (GrandPré et al., 2002), arguing either that both Nogo-66 and Amino-Nogo have a role in myelin inhibition or that pharmacologic blockade is less than 100% effective for Nogo-66. Similar results were observed in postnatal mouse cerebellar neurons and in adult mouse DRG cultures (Figure 3D). At high concentrations, it is clear that *nogo-A/B*$^{-/-}$ myelin possesses inhibitory activity. We considered whether this might be attributable to MAG. Residual myelin inhibitory activity is blocked by anti-MAG antibodies (Figure 3E). Thus, Nogo-A, and secondarily MAG, accounts for a majority of axon inhibitory activity in CNS myelin preparations.

Corticospinal Tract Sprouting after SCI in *nogo-A/B*$^{-/-}$ Mice

To consider what effect the lack of myelin-dependent axon inhibition might have on axonal regeneration after CNS axotomy, we performed dorsal hemisection injuries at T6 in *nogo-A/B*$^{-/-}$ mice. The descending corticospinal tract (CST) was visualized by cortical biotin-dextran amine (BDA) injections (Figures 5A–5E). Tissue was collected 18–21 days after SCI. In wild-type littermate mice (data not shown) or in *nogo-A/B*$^{+/-}$ control mice, the dorsal CST (dCST) is tightly bundled at the base of the contralateral dorsal columns rostral to the lesion site at T3 (Figures 4A and 4B). A smaller percentage (~3% or 15/mouse) of CST fibers are observed in the crossed dorsolateral CST (dlCST) and uncrossed ventral CST (vCST; ~0.5% or 2/mouse). A dramatically different pattern is seen rostral to the spinal cord hemisection in the littermate *nogo-A/B*$^{-/-}$ mice (Figures 4B and 4D). The dCST is normally positioned, but numerous CST fibers are detected in the lateral funiculus on the side ipsilateral to the cortical BDA injection. The total number of fibers outside of the dCST is increased nearly 10-fold in the *nogo-A/B*$^{-/-}$ mice (Figure 4F). More specifically, the number of fibers ipsilateral to the injection is increased nearly 100-fold in the absence of Nogo-A. All 8 of 8 control mice of 7.5–9 weeks of age at the time of injury had three or fewer CST fibers in the lateral funiculus ipsilateral to the injection site, while 12/12 of similarly

aged *nogo-A/B*$^{-/-}$ mice had greater than this number, with an average of 117 fibers. Only three older (11–14 weeks at injury) *nogo-A/B*$^{-/-}$ mice were examined, but there was a trend to less pronounced sprouting, with an average of seven ectopic fibers per animal. Mice of both age groups are included in the statistical analysis (Figure 4F). Densitometric analysis confirmed the elevation of BDA labeling in the ipsilateral lateral funiculus (Figure 4G).

The ipsilateral fibers observed in the hemisected *nogo-A/B*$^{-/-}$ mice might reflect a developmental malformation or a response to injury. To assess this possibility, BDA was injected into uninjured mice and the CST was traced. The uninjured *nogo-A/B*$^{-/-}$ mice exhibit a trend toward increased contralateral fibers outside of the dCST, but this does not reach statistical significance (Figure 4F). Clearly, the 100-fold increase in CST fibers in the lateral cord ipsilateral to the cortical injection occurs only with the combination of injury plus the *nogo-A/B*$^{-/-}$ mutation. These fibers might derive from descending fibers that sprout at the pyramidal decussation and then traverse the ipsilateral cord in a direct path, or from collaterals of the dCST that preferentially recross the midline to assume a position ipsilateral to the BDA injection. Examination of the medulla and the pyramidal decussation at the cervicomedullary junction does not reveal any obvious abnormality in the hemisected *nogo-A/B*$^{-/-}$ mice (data not shown). Instead, there is a gradual increase in the number of ectopic CST fibers in a progression from rostral to caudal in the spinal cord, with greatest numbers near the injury site (Figure 4H). While single fibers could not be traced for long distances in these preparations, the simplest explanation for the observed CST fibers is a steady increase in collateral sprouting closer to the axotomy site with a preference of sprouted fibers to recross the spinal cord. A number of CST fibers can be seen crossing the midline immediately dorsal to the central canal of the spinal cord in hemisected *nogo*$^{-/-}$ mice rostral to the injury (Figure 4E). The data demonstrate a pronounced CNS axonal sprouting response to injury in the *nogo-A/B*$^{-/-}$ mice.

Corticospinal Axon Regeneration after SCI in *nogo-A*$^{-/-}$ Mice

While CST fibers sprout extensively above a thoracic hemisection in *nogo-A/B*$^{-/-}$ mice, a more critical issue is whether such fibers project to the caudal spinal cord below the injury. Examination of longitudinal sections across the SCI demonstrate that many fibers do regenerate across the injury site and can be seen to follow a branching trajectory in distal gray and white matter (Figures 5A and 5B). The tortuous trajectory is distinct from rostral fibers in control animals, which have a linear profile in the dCST (Figures 5E and 5F). It is also clearly distinct from the linear trajectory of caudal uninjured fibers in wild-type animals with a more shallow injury that does not disrupt the entire dCST (not seen in this study but observed in pilot experiments; data not shown). As further validation of the extent of the transection, staining for the astroglial marker, GFAP, demonstrates that scar reaches deeper than the level of the dCST (Figures 5C and 5D). Camera lucida drawings of all BDA-labeled fibers summarize the pattern of CST fiber growth in the rostral-caudal region of the injury (Figures 5E–5K). No dCST fibers extend past a dorsal hemisection in wild-type or *nogo-A/B*$^{+/-}$ mice (Figures 5E and 5F). In five *nogo-A/B*$^{-/-}$ mice, the pattern of CST fiber sprouting around and past the lesion is extensive (Figures 5G–5K).

Regenerating CST fibers are seen in transverse spinal cord sections more than 5 mm caudal to the hemisection (Figure 6). While occasional uninjured vCST or lateral fibers are seen in hemisected wild-type or *nogo-A/B*$^{+/-}$ mice at this level, the average CST axon number is 40-fold greater in the *nogo-A/B*$^{-/-}$ mice, and 7 of 11 mice of 7.5–9 weeks at injury exhibited fiber counts outside the range of control mice (Figure 6F). A majority of the regenerating CST fibers in Nogo-A null mice are detected bilaterally in the lateral white matter of the cord (Figures 6B and 6D). Few or no regenerating fibers are observed in the normal position of the CST, the dorsal column. Densitometric analysis of HRP labeling of BDA-containing fibers in the lateral columns confirms the increased axon number in the *nogo-A/B*$^{-/-}$ mice (Figure 6G). Three *nogo-A/B*$^{-/-}$ mice underwent surgery at 11–14 weeks of age. In this small group, proximal sprouting was less prominent and no CST fibers regenerated to a distance 5 mm below the injury site (Figure 6F). Overall, long-distance axonal regeneration is prominent in a majority of the *nogo-A/B*$^{-/-}$ mice examined.

Improved Locomotor Recovery after SCI in *nogo-A/B*$^{-/-}$ Mice

We considered whether the extensive long-distance axonal regeneration in the *nogo-A/B*$^{-/-}$ mice is correlated with functional recovery after this midthoracic dorsal hemisection injury. Recovery was assessed using a standardized open-field measure of locomotor function after SCI, the BBB score. In this scale, 21 is normal function and 0 is bilateral total paralysis of the hindlimbs. All mice had scores of 3 or less at 4 hr post injury (data not shown). The *nogo-A/B*$^{+/-}$ mice gradually recover partial function over a 21-day observation period (Figure 6H). The BBB scores of *nogo-A/B*$^{-/-}$ mice are significantly higher than controls throughout the 2–21 day period. While it is possible that the early (2 day) improvement is due to some long-distance growth of CST fibers extending from the lesion site to the lumbar motor pool, it seems much more probable that this is due to short-range sprouting of partially injured tracts such as the raphespinal system in the ventrolateral portions of the cord (see Discussion). At the 17-day time point, the higher scores of *nogo-A/B*$^{-/-}$ mice might be attributable to both the long-distance CST regeneration seen by BDA tracing and to local sprouting in the lumbar cord. By this time point, functional recovery from dorsal hemisection is nearly complete (GrandPré et al., 2002). Regardless of mechanism, the locomotor recovery in the *nogo-A/B*$^{-/-}$ mice is significantly greater than in control animals.

Discussion

Analysis of mice with a disruption in the *nogo-A/B* gene has provided insights into the response of young adult brain and spinal cord to trauma. The hypothesis that

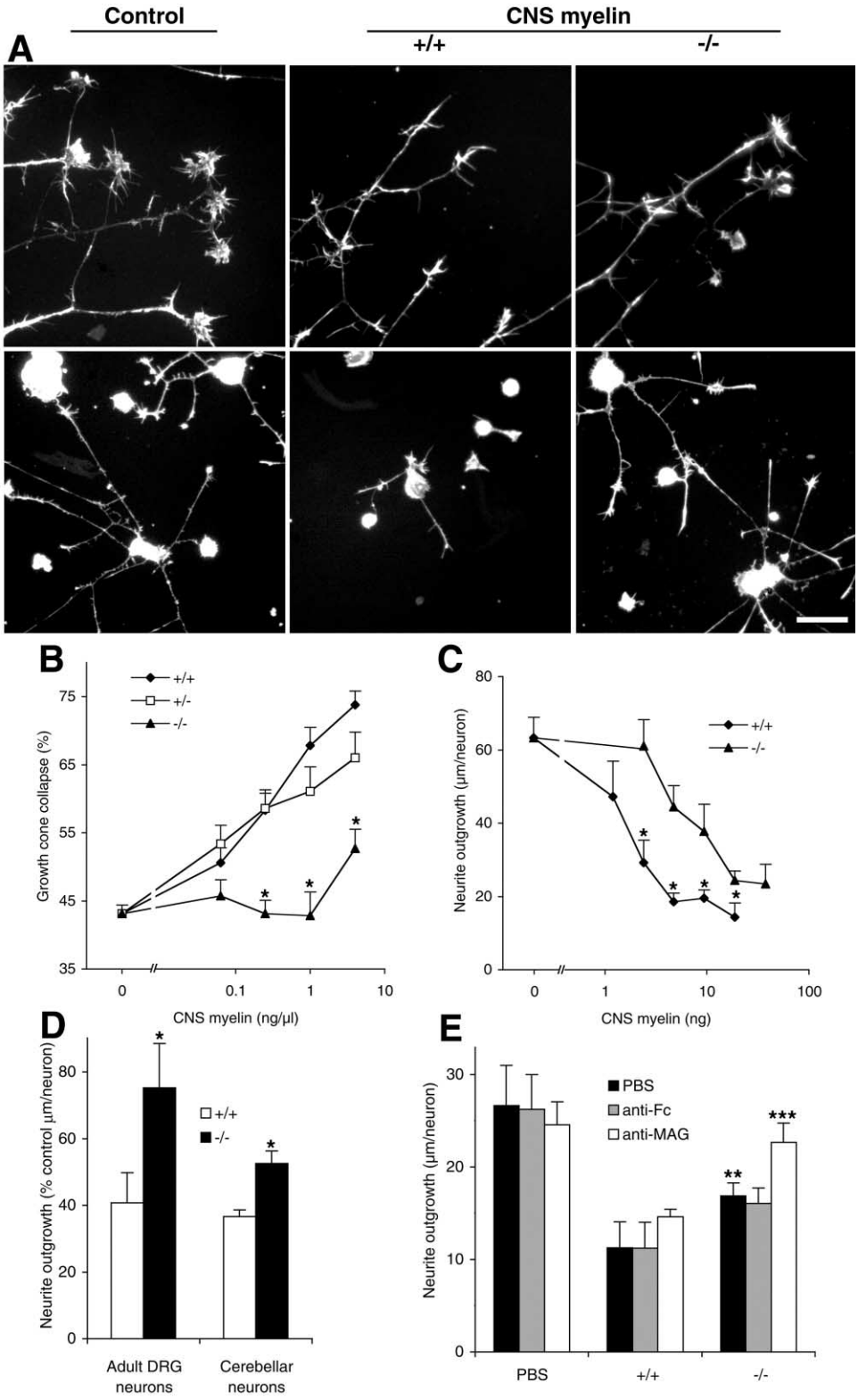

Figure 3. Growth Cone Collapse and Neurite Outgrowth Assays Using Nogo-A/B-Deficient Myelin

(A) Growth cone collapse (upper panels) and neurite outgrowth (lower panels) assays. E12 chick DRG explants were treated with 1 ng/μl CNS myelin purified from either *nogo-A/B*$^{+/+}$ or *nogo-A/B*$^{-/-}$ brains for 30 min. Dissociated E12 chick DRG neurons were plated on dried spots of CNS myelin (2 ng) purified from either *nogo-A/B*$^{+/+}$ or *nogo-A/B*$^{-/-}$ brains and incubated 5–7 hr. Scale bar equals 25 μm for upper panels and 50 μm for lower panels.

myelin-derived Nogo-A participates in limiting CNS axon regeneration is supported by several lines of evidence presented here. CNS myelin has greatly reduced in vitro axon inhibitory activity. Most importantly, after SCI, numerous axonal sprouts are observed in the spinal cord and long-distance CST regeneration is prominent. It appears that Nogo-A plays a role in regulating axonal sprouting and plasticity in the young adult CNS. However, uninjured brain structure and function is largely normal in the *nogo-A/B*$^{-/-}$ mice.

Axonal Sprouting after Axotomy in the *nogo-A/B*$^{-/-}$ Mice

In the adult mammalian CNS, injured axons exhibit little if any sprouting. In the *nogo-A/B*$^{-/-}$ young adult mice, the CST sprouts exuberantly after injury even though its morphology appears normal in uninjured animals. Based on the in vitro inhibitory activity of Nogo-66 via an axonal NgR (GrandPré et al., 2000; Fournier et al., 2001), the simplest explanation would appear to be that Nogo-A in wild-type oligodendrocytes inhibits axonal growth after injury. An alternative speculation based on a role for neuronal Nogo-A seems implausible since there is no clear in vitro correlate and since neuronal Nogo-C expression remains high in the *nogo-A/B*$^{-/-}$ mice and might be expected to produce compensatory effects. However, genetic modifiers of the effects of oligodendrocyte Nogo-A deficiency may exist (see accompanying papers Zheng et al., 2003; Simonen et al., 2003 [in this issue of *Neuron*]). Since axonal CST sprouting does not occur in the absence of injury, an unidentified axotomy signal that has the capacity to induce a sprouting response must be suppressed by Nogo-A signaling under normal conditions. In a CNS devoid of Nogo-A or in a peripheral nerve transplant, this signal becomes capable of exerting its positive effect on axonal growth.

Long-Distance Axonal Regeneration in the *nogo-A/B*$^{-/-}$ Mice

Axonal sprouting is associated with long-distance regeneration of CST axons in the *nogo-A/B*$^{-/-}$ mice. Hundreds of CST fibers are detectable millimeters caudal to the injury site of mutant mice within weeks of a SCI. This degree of axonal regeneration compares favorably to olfactory ensheathing cell transplant studies (Ramón-Cueto et al., 2000). Perhaps not surprisingly, the extent of regeneration exceeds that achieved by pharmacologic or immunologic blockade of Nogo action (GrandPré et al., 2002; Bregman et al., 1995; Hauben et al., 2001). This might be due to the mutation altering both Amino-Nogo and Nogo-66 function in oligodendrocytes. While other limitations to axonal regeneration might exist in the adult CNS, it is clear that perturbation of the *nogo* gene is sufficient to allow a degree of axonal regeneration. This study considers only SCI and CST axons; no other axons are considered. However, given the widespread distribution of Nogo in oligodendrocytes and NgR in adult neurons (GrandPré et al., 2000; Fournier et al., 2001; Wang et al., 2002a; Huber et al., 2002), it seems likely that the regeneration of numerous other pathways are subject to similar limitation by Nogo-A. We speculate that other axonal pathways would exhibit long-distance regeneration after injury in the absence of Nogo-A.

All young adult *nogo-A/B*$^{-/-}$ mice exhibited pronounced CST axon sprouting proximal to the injury. Preliminary studies indicate that sprouting may be restricted at older ages in the *nogo-A/B*$^{-/-}$ mice. Further experiments are required to determine if there is a "critical period" for robust axon regeneration in the *nogo-A/B*$^{-/-}$ mice.

Other Axon Regeneration Inhibitors

Among myelin constituents, Nogo-A accounts for the vast majority of axon inhibition in vitro, based on the results presented here. CNS myelin lacking Nogo-A inhibits axon outgrowth in vitro weakly but is only about one-eighth as potent as wild-type myelin. The residual axon inhibitory activity in *nogo-A/B*$^{-/-}$ myelin may be due to MAG, OMgp, and/or CSPGs. Anti-MAG antibody experiments with *nogo-A/B*$^{-/-}$ myelin support a role for both Nogo-A and MAG in vitro. Nonmyelin CNS components, such as astrocyte scar-derived CSPGs, contactin, and Sema3A, have been implicated as CNS axon regeneration inhibitors based on various assays (reviewed by Fournier and Strittmatter, 2001; Fawcett and Asher, 1999). The relative contribution of these molecules is not considered here, but it is clear that a degree of CST axon growth can occur in young adult *nogo-A/B*$^{-/-}$ mice capable of expressing these other factors. Perhaps such nonmyelin factors require Nogo-A function synergistically to limit axonal regeneration by a multifactorial mechanism. Loss of either Nogo-A function or that of nonmyelin axon regeneration inhibitors might allow extensive axonal regeneration. Such a notion is supported by recent results with chondroitinase ABC delivery to SCI sites (Bradbury et al., 2002) and by microtransplant studies (Davies et al., 1999). There is also preliminary evidence that age may affect sprouting. In the *nogo-A/B*$^{-/-}$ mice, CST sprouting may occur only when SCI occurs at the young adult stage.

Guidance of Regenerating Axons

The CST exhibits both collateral sprouting rostral to the cord lesion and long-distance growth into caudal cord

(B) Quantitation of growth cone collapse in E12 chick DRG explants treated with soluble myelin extracts derived from brains of *nogo-A*$^{+/+}$, *nogo-A*$^{+/-}$, and *nogo-A/B*$^{-/-}$ mice.
(C) Quantitation of neurite outgrowth in dissociated E12 chick DRG neurons plated on dried spots of myelin extracts derived from brains of *nogo-A/B*$^{+/+}$ and *nogo-A/B*$^{-/-}$ mice.
(D) Neurite outgrowth from adult mouse DRG or P8 cerebellar neurons placed on spots of myelin from *nogo-A/B*$^{+/+}$ or *nogo-A/B*$^{-/-}$ mice (DRG, 2 ng myelin, cerebellar, 35 ng myelin).
(E) Neurite outgrowth from chick E12 DRG cultured on 10 ng spots of myelin from *nogo-A/B*$^{+/+}$ or *nogo-A/B*$^{-/-}$ mice in the presence of PBS, 25 μg/ml control IgG, or 25 μg/ml of anti-MAG.
All data are represented as mean ± SEM. Single asterisk, significantly different from wild-type, $p \leq 0.01$; double asterisk, significantly different from wild-type/PBS, $p \leq 0.05$; triple asterisk, significantly different from −/− PBS, $p \leq 0.05$ (Student's t test).

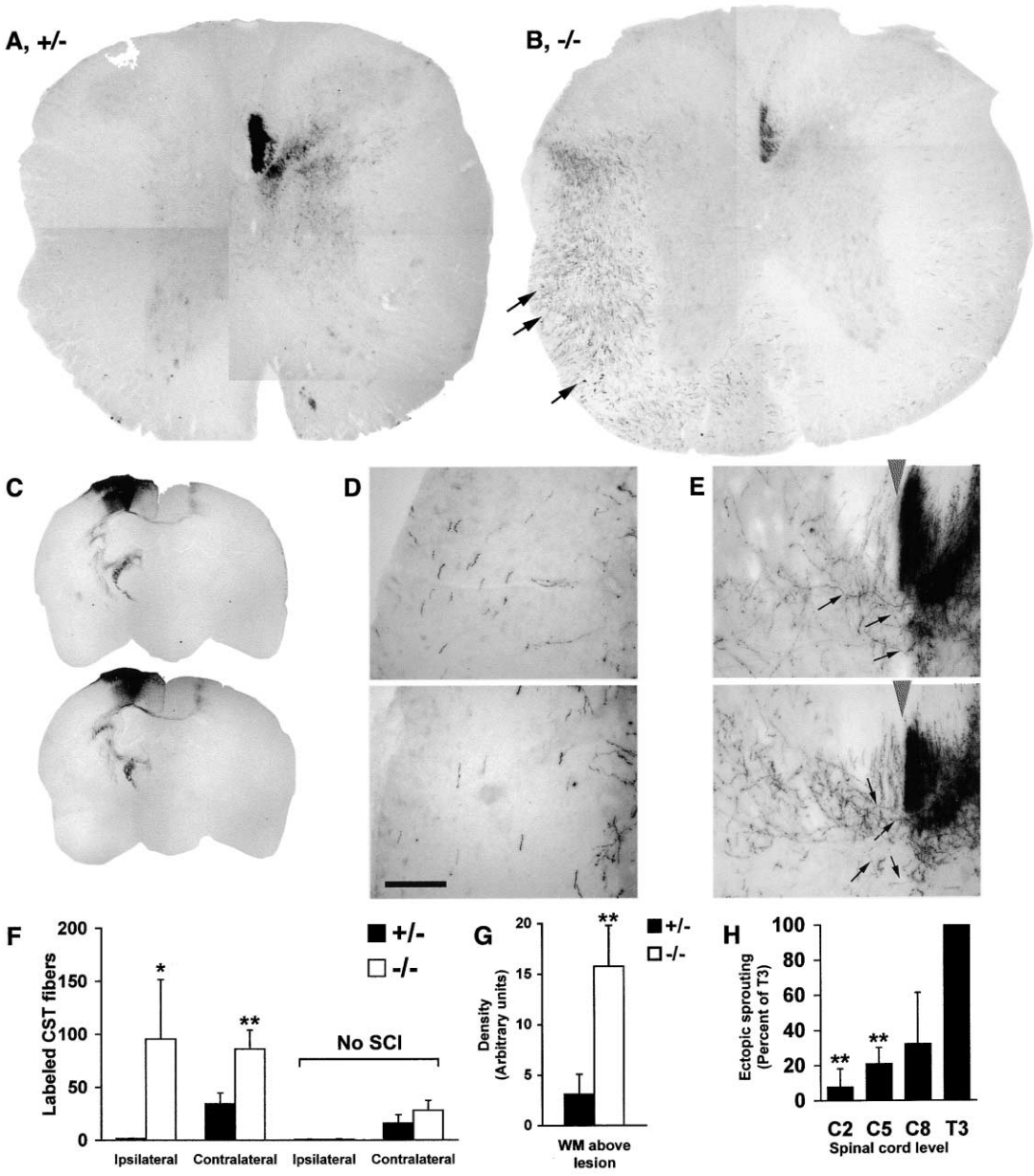

Figure 4. CST Fiber Sprouting Rostral to the Lesion in *nogo-A/B*$^{-/-}$ Mice

(A and B) T3 crosssections of spinal cord from *nogo-A/B*$^{+/-}$ and *nogo-A/B*$^{-/-}$ mice, respectively, 21 days post injury 5 mm rostral to the transection. The BDA-injected cerebral cortex corresponds to the left of these sections, so the major crossed dCST is on the right. Arrows indicate ectopic CST fibers ipsilateral to the injection site in (B).

(C) Coronal sections of the BDA injection site from two *nogo-A/B*$^{-/-}$ mice. The left cerebral cortex injection and projections to the capsular system and across the corpus callosum to the contralateral hemisphere are visualized. Spinal cord segments from the same animals are shown in (D) and (E).

(D) Labeled CST fibers in lateral funiculus ipsilateral to the BDA injection from two *nogo-A/B*$^{-/-}$ mice. Scale bar equals 100 μm (D and E).

(E) Labeled CST fibers near the midline of the spinal cord and 5 mm rostral to a hemisection from two *nogo-A/B*$^{-/-}$ mice. The heavily labeled contralateral dCST is seen to the right of the midline (gray arrowhead). The arrows indicate CST fibers crossing the midline in the gray matter ventral to the dorsal columns.

(F) Labeled lateral column CST fibers 5 mm rostral to lesion ipsilateral or contralateral to the BDA injection with or without SCI in *nogo-A/B*$^{+/-}$ (n = 8) and *nogo-A/B*$^{-/-}$ (n = 15) mice. Single asterisk, values significantly different from corresponding +/− value.

(G) The optical density of HRP labeling of BDA-traced CST fibers in the lateral columns from sections such as (A) and (B).

(H) Ectopic CST sprouting outside the dCST in *nogo-A/B*$^{-/-}$ mice at different levels of the spinal cord. Single asterisk, values significantly different from T3 value.

All data are represented as mean ± SEM. Significance, *$p \leq 0.05$; **$p \leq 0.01$ versus control (Student's t test).

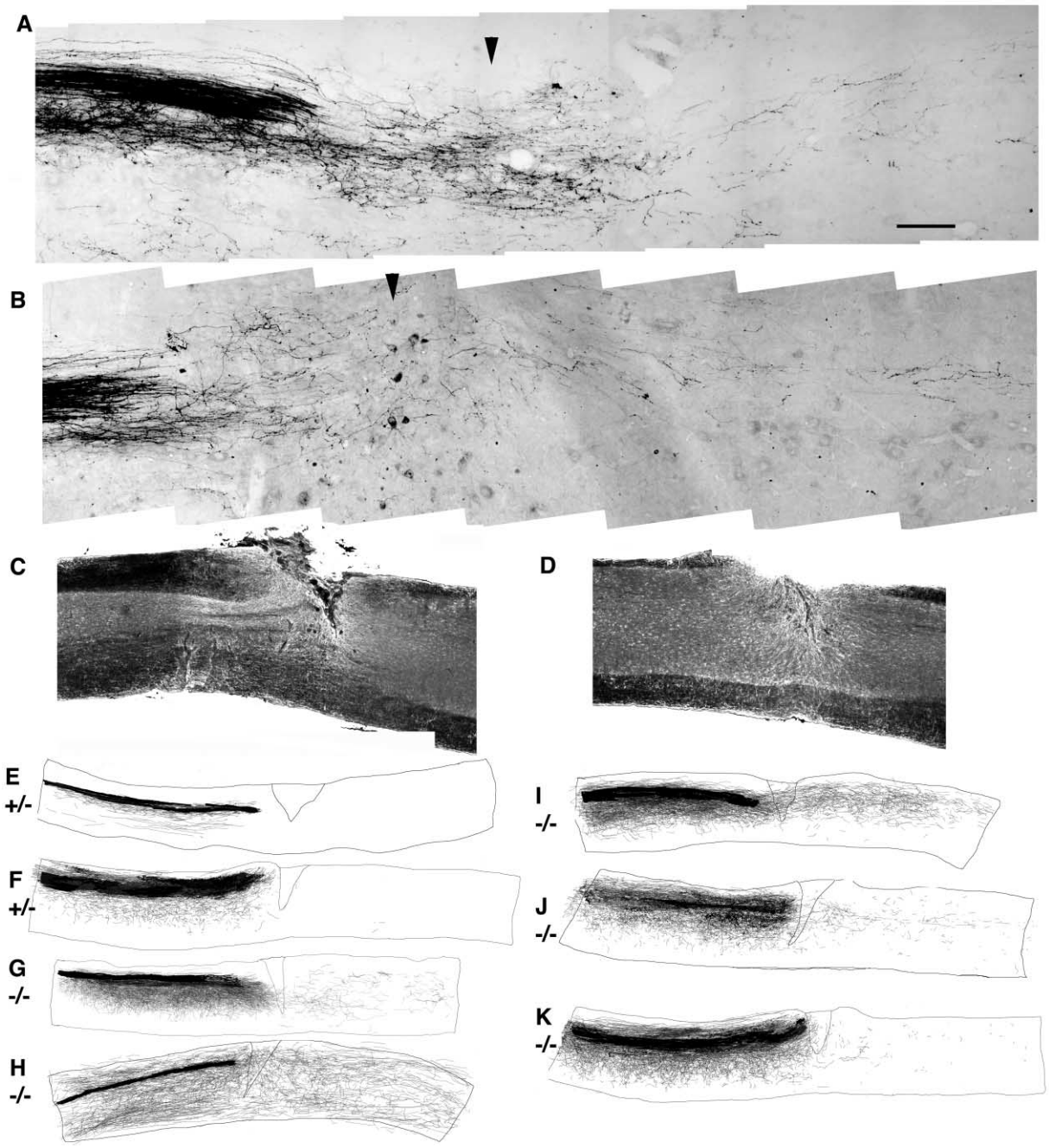

Figure 5. Long-Distance CST Regeneration and Sprouting in Nogo-A/B Knockout Mice

(A and B) Parasagittal sections of spinal cord containing lesion sites (arrowheads) in two different *nogo-A/B*$^{-/-}$ mice. Numerous branching axons extend into the caudal spinal cord segment. Minor cavitation and phagocytic cells in the lesion site are seen. Rostral is to the left and dorsal is up. Scale bar equals 200 μm.

(C and D) Parasagittal sections demonstrating GFAP staining around the injury site in two *nogo-A/B*$^{-/-}$ mice.

(E–K) Camera lucida drawings of all BDA-labeled CST axons in all consecutive parasagittal sections from a 1 cm section of the thoracic spinal cord containing the hemisection. The genotype of the mice is indicated. Based on the transverse section data of Figure 6 below, many of the caudal fibers are present in lateral white matter regions.

segments in the *nogo-A/B*$^{-/-}$ mice. While the overall trajectory of this growth appears to be caudal, the CST is remarkably different than in its preinjury state. Above the hemisection, most collateral CST fibers project across the midline and assume a nonfasciculated lateral position in the white matter. This crossing reverses the pyramidal decussation that CST axons create during the late embryonic period, so that many CST fibers are seen ipsilateral to the cortical injection site. The molecular cues driving collateral CST sprouts to recross the midline in hemisected *nogo-A/B*$^{-/-}$ mice have not been delineated. The L1 adhesion molecule has a role in creat-

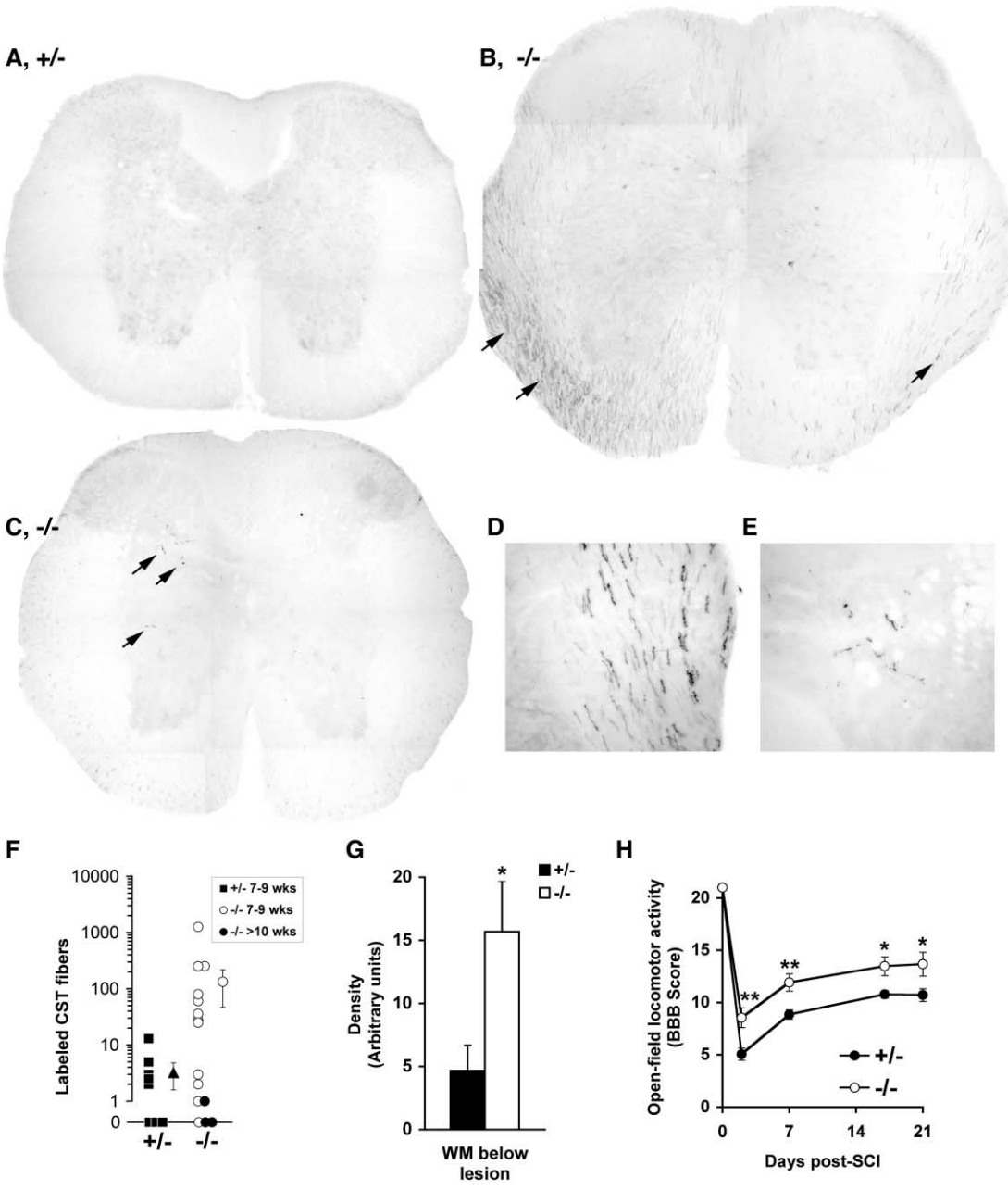

Figure 6. CST Fiber Sprouting Below the Lesion and Improved Functional Recovery in Nogo-A/B Knockout Mice

(A–C) Crosssections of spinal cord at L1 from *nogo-A/B*$^{+/-}$ and *nogo-A/B*$^{-/-}$ mice, 21 days post-SCI. Arrows indicate labeled CST fibers in (B) and (C).

(D) Labeled CST fibers in lateral white matter from a *nogo-A/B*$^{-/-}$ mouse.

(E) Labeled CST fibers in gray matter from a different *nogo-A/B*$^{-/-}$ mouse than in (D).

(F) Quantitation of labeled CST fibers found in white and gray matter from *nogo-A/B*$^{+/-}$ (n = 8) and *nogo-A/B*$^{-/-}$ mice (n = 15), 5 mm caudal to lesion.

(G) The optical density of HRP labeling of BDA-traced CST fibers in the lateral columns from sections such as (A)–(C).

(H) Comparison of open-field locomotor activity in *nogo-A/B*$^{+/-}$ (n = 19) and *nogo-A/B*$^{-/-}$ (n = 20) mice. All data are represented as mean ± SEM. Single asterisks indicate $p < 0.05$ and double asterisks indicate $p < 0.001$ versus *nogo-A/B*$^{+/-}$ (Student's t test).

ing the pyramidal decussation during development of the mouse and human CNS (Cohen et al., 1998), but it does not appear to function in maintaining laterality within the cord. While both the Slit and Netrin proteins have prominent roles in midline repulsion and attraction for other pathways, they are not known to regulate CST growth in the spinal cord. However, there is clear evidence that EphA4 receptors on CST axons respond to a spinal cord midline Ephrin B3 barrier to prevent CST recrossing during development (Kullander et al., 2001; Leighton et al., 2001; Yokoyama et al., 2001). It is not known whether EphA4 and Ephrin B3 are expressed in

fully mature or injured spinal cord. It seems plausible that either EphA4 or Ephrin B3 is downregulated and that this fact contributes to collateral CST fiber recrossing in injured *nogo-A/B*$^{-/-}$ mice.

Below the hemisection, regenerating CST fibers follow highly branched and perhaps random courses, populating both gray and white matter throughout the cord. Here, axonal guidance is only apparent in the overall caudal course of fibers. There is no evidence for topographic organization within the cord, so that this aspect of developmental axon guidance is not recapitulated during long-distance regeneration of the CST in Nogo-A-deficient spinal cord. It is also notable that the caudal fibers regenerating from the injured end of the CST axon do not follow the same recrossing trajectory as do the rostral collateral sprouts. Of course, guidance to and synapse formation with the appropriate lumbar motoneurons is the most critical aspect of axon guidance. While some BDA-labeled synapse-like profiles in the lumbar ventral horn were observed in this study (data not shown), investigation of this issue will require topographic mapping of multiple discrete groups of regenerating fibers in chronically injured *nogo-A/B*$^{-/-}$ mice combined with ultrastructural analysis.

Functional Recovery of Locomotion after SCI

After midthoracic dorsal hemisection, wild-type mice recover a proportion of open-field locomotor performance over several weeks. This recovery is accelerated in *nogo-A/B*$^{-/-}$ mice and is most dramatic at times as early as 2 days post injury. Most likely, increased axonal growth is responsible for the improved locomotor scores. It is not as clear which fiber tracts are responsible. The dCST does exhibit long-distance regeneration, and this might possibly contribute to functional locomotor recovery during the 1–3 week period. However, at 2 days post injury, the functional improvement is likely to be due instead to collateral sprouting in the lumbar cord from other, partially injured, tracts. This argument is based in part on the fact that regeneration under optimal circumstances in the sciatic nerve proceeds at 2 mm/day, and the distance from the hemisection to the lumbar motor pool is 5–10 mm in these animals. The raphespinal system is widely distributed in the cord and is only partially injured in the hemisection model (Bregman et al., 1995; Saruhashi et al., 1996; GrandPré et al., 2002). A role for the raphespinal system in locomotor pattern generation has been documented (Saruhashi et al., 1996), and both IN-1 antibodies (Bregman et al., 1995; Bandtlow and Schwab, 2000) and NgR peptide antagonists (GrandPré et al., 2002) promote 5-HT fiber sprouting. Furthermore, similar early improvement in BBB scores after dorsal hemisection have been also observed in studies with IN-1 antibodies (Merkler et al., 2001) and with NgR peptide antagonist (GrandPré et al., 2002). Therefore, collateral sprouting of the raphespinal system in the distal cord is a plausible mechanism for the early recovery of *nogo-A/B*$^{-/-}$ mice. Rearrangements of other descending tracts, such as the rubrospinal system, or of distal intrinsic spinal cord circuitry might also contribute.

Conclusions

Nogo-A appears to be a signficant axon growth inhibitor in young adult CNS myelin. In the mice with a mutation in the *nogo* gene that prevents Nogo-A/B expression, the nervous system is largely normal but responds to injury in a unique fashion, with robust axonal sprouting and long-distance growth. While Nogo-A/B deficiency is partially responsible for the effect of this mutation, other uncharacterized genetic factors may influence its expression (see accompanying papers Zheng et al., 2003; Simonen et al., 2003). Axon guidance for regenerating fibers is clearly not as precise as for developing fibers. Nonetheless, spinal-injured *nogo-A/B*$^{-/-}$ mice perform better in the open field than do control mice.

Experimental Procedures

Generation and Maintenance of Nogo-A/B Mutant Mice

A *nogo*-targeted embryonic stem (ES) cell clone was identified from the OmniBank Sequence Tag database (OST 45048, Lexicon Genetics, Inc.). The OmniBank mutations are created using insertional mutagenesis based on retroviral-based gene trap methodology (Zambrowicz et al., 1998). Heterozygotic mice harboring the disrupted allele were bred to C57 Bl/6 mice for colony expansion in our animal housing facility and intercrossed to maintain the *nogo-A/B* mutation on a hybrid 129/SvEvBrd × C57 Bl/6 background. In the experiments here, animals had been backcrossed to C57BL/6 for 3–6 generations and 7- to 14-week-old *nogo-A/B*$^{+/+}$ or *nogo-A/B*$^{+/-}$ littermates were used as controls for all experiments. In all in vitro and behavioral assays, investigators were unaware of the mouse genotypes at the time of measurements.

Southern and Northern Analyses

For Southern blot analysis, tail DNA was extracted using the DNeasy Tissue Kit (Qiagen). Ten micrograms of DNA was digested with Nhe I, electrophoresed into an agarose gel, and blotted onto a nylon membrane. After UV-crosslinking, the membrane was hybridized with random-primed ^{32}P-labeled *nogo* probes at 42°C in a 50% formamide/5× SSPE/10% dextran sulfate/1% SDS solution and washed at 62°C with 0.1× SSC/0.1% SDS. Genotypic screening was performed by PCR (*nogo-A*-specific forward primer, 5′-ATTATG GATTTGATGGAGCAGCCAGGTAAC-3′; *nogo-A*-specific reverse primer, 5′-CATCTGTTTTGTTTTCTGAAGTGTGATCTTC-3′; virus-specific reverse primer, 5′-CAAGGAAACCCTGGACTACTGCGC-3′).

For Northern blots, total brain RNA was isolated using the RNeasy Midi Kit (Qiagen). Thirty micrograms of total RNA was separated on a 1% agarose/2% formaldehyde/1× MOPS gel, blotted to a nylon membrane, UV-crosslinked, and hybridized using ^{32}P-labeled probes. The 5′ *nogo-A* probe corresponds a region in exon 1 encoding aa 30–145. The 3′ *nogo* probe corresponds to a *nogo-A* cDNA sequence encoding aa 1013–1162 and detects all endogenous *nogo* isoforms equally. The *ngr* probe is from a full-length mouse cDNA. Hybridization was performed using the NorthernMax™ kit according to the manufacturer's instructions (Ambion).

Immunoblotting

Brain or lung tissue was homogenized in RIPA buffer (1% Triton X-100/0.5% sodium deoxycholate/0.1% SDS/1× PBS) supplemented with 1× protease inhibitor cocktail mix (Roche) and sonicated, and the supernatant was collected after centrifugation. Myelin protein was prepared (Norton and Poduslo, 1973) and extracted with 2% octylglucoside before dialysis against PBS. Thirty micrograms of brain lysate or seven micrograms of myelin extract was separated by SDS-PAGE and blotted onto PVDF. Affinity-purified rabbit antibodies against Nogo-A was used at 50 ng/ml (Wang et al., 2002a), and antibodies detecting an amino-terminal peptide of Nogo-A/B were diluted to 400 ng/ml (N-18; Santa Cruz Biotechnologies). Goat anti-MAG (Sigma) and rabbit anti-MBP (Zymed) antibodies were diluted 1:1000 and 1:10, respectively. Immunoreactivity was visualized after incubation with biotinylated secondary antibod-

ies and avidin-AP (Vector Laboratories) using NBT/BCIP AP substrates.

Growth Cone Collapse and Neurite Outgrowth Assays

E12 chick DRG, adult mouse DRG, and P8 cerebellar granule cell outgrowth assays have been described (GrandPré et al., 2000). For growth cone collapse assays, DRG explants on plastic slides precoated with 100 μg/ml poly-L-lysine and 10 μg/ml laminin were cultured for 14–16 hr prior to treatment for 30 min with soluble CNS myelin extracts. Myelin preparation is described above. For neurite outgrowth assays, plastic chamber slides were coated with 100 μg/ml poly-L-lysine, washed, and dried. Three microliter drops of PBS containing CNS myelin were spotted and dried. Slides were then rinsed and coated with 10 μg/ml laminin before addition of dissociated E12 chick DRGs. Cultures were incubated for 5–7 hr before neurite outgrowth was assessed. In some cultures, rabbit anti-MAG antibodies (Chemicon) or control IgG were added prior to cell plating at 25 μg/ml.

Behavioral Analysis

To assess open-field activity, mice were acclimated for at least 30 min and then placed in the mouse activity-monitoring cage (Coulbourn Instruments) for 15 min. Floor plane sensor measurements were collected using Tru Scan 99 software for a total of three sessions performed on three consecutive days. To assess locomotor coordination, mice were first trained on the rotarod (Technical Scientific Equipment) at the lowest speed setting (2–10 rpm) for six sessions on 2 consecutive days. Performance on the mid-range speed setting (3–15 rpm) with acceleration was recorded for three 10 min sessions on 4 consecutive days for a total of 12 sessions.

Following SCI, the BBB scale was used to assess open-field locomotor deficits (Basso et al., 1996). Two animals, one from the *nogo-A/B*$^{+/-}$ group and the other from *nogo-A/B*$^{-/-}$, were excluded from the study, as they had declining scores in the second postoperative week and evidence of dehydration, likely secondary to infection.

Spinal Cord Dorsal Hemisection and Corticospinal Fiber Tracing

All surgical procedures and postoperative care was performed in accordance with guidelines of the Yale Animal Care and Use Committee. Female mice were deeply anesthesized with intraperitoneal ketamine (100 mg/kg) and xylazine (15 mg/kg). Laminectomies were perfomed at spinal levels T6 and T7, exposing the spinal cord. A dorsal hemisection was performed at T6 using the tip of a 32-gauge needle, completely interrupting the dorsal and dorsolateral CSTs. The muscle layers over the laminectomies were sutured, and the skin on the back was closed with surgical staples. For tracing the corticospinal tract, the scalp was cut, and a hole was drilled into the skull overlying the sensorimotor cortex. By four injections, 1.5 μl of the biotin dextran amine (BDA, MW 10,000; 10% in PBS, Molecular Probes) was applied. The scalp was closed with surgical staples. Ampicillin was administered intramuscularly twice daily for 3 days postoperatively, and the bladder was expressed by massage three times a day for the entire duration of survival.

Histology and Analysis

Animals were perfused transcardially with PBS followed by a 4% paraformaldehyde/PBS solution. Spinal cords were dissected, postfixed overnight, and embedded in a glutaraldehyde-polymerized albumin matrix for vibratome sectioning or flash-frozen in Tissue Freezing Medium (TBS) for cryostat sectioning. Fifty-micrometer-thick free-floating sections were preincubated with 0.5% BSA/TBS and then processed with avidin-HRP (Elite ABC, Vector Laboratories) followed by a nickel-enhanced diaminobenzidine reaction. The sections were mounted, dehydrated, and coverslipped with DPX mounting medium (BDH Laboratory Supplies). For fiber counts, sections were examined with a 20× objective lens. For camera lucida drawing, all consecutive parasagittal were imaged and BDA-positive CST axons were traced from 5 mm above to 5 mm below the injury site. Densitometric measurements of HRP staining of BDA containing lateral funicular fibers were obtained from digital images of transverse spinal cord sections with a 4× objective.

Acknowledgments

We thank Marc Tessier-Lavigne and Martin Schwab for sharing unpublished results, Michael Schwartz for assistance with open-field behavior and rotarod measurements, and Xiaofang Yang for technical assistance. This work was supported by research grants to S.M.S. from the NIH, the McKnight Foundation, the Institute for the Study of Aging, and Biogen, Inc. T.G. is a Bayer Predoctoral Scholar, and S.M.S. is an Investigator of the Patrick and Catherine Weldon Donaghue Medical Research Foundation.

Received: May 7, 2002
Revised: January 27, 2003
Accepted: March 13, 2003
Published: April 23, 2003

References

Bandtlow, C.E., and Schwab, M.E. (2000). NI-35/250/nogo-a: a neurite growth inhibitor restricting structural plasticity and regeneration of nerve fibers in the adult vertebrate CNS. Glia *29*, 175–181.

Bandtlow, C.E., Zachleder, T., and Schwab, M.E. (1990). Oligodendrocytes arrest neurite growth by contact inhibition. J. Neurosci. *10*, 3837–3848.

Bartsch, U., Bandtlow, C.E., Schnell, L., Bartsch, S., Spillmann, A.A., Rubin, B.P., Hillenbrand, R., Montag, D., Schwab, M.E., and Schachner, M. (1995). Lack of evidence that the myelin-associated glycoprotein (MAG) is a major inhibitor of axonal regeneration in the CNS. Neuron *15*, 1375–1382.

Basso, D.M., Beattie, M.S., and Bresnahan, J.C. (1996). Graded histological and locomotor outcomes after spinal cord contusion using the NYU weight-drop device versus transection. Exp. Neurol. *139*, 244–256.

Benfey, M., and Aguayo, A.G. (1982). Extensive elongation of axons from rat brain into peripheral nerve grafts. Nature *296*, 150–152.

Bonilla, I.E., Tanabe, K., and Strittmatter, S.M. (2002). SPRR1A is expressed by axotomized neurons and promotes axonal outgrowth. J. Neurosci. *22*, 1303–1315.

Bradbury, E.J., Moon, L.D.F., Popat, R.J., King, V.R., Bennett, G.S., Patel, P.N., Fawcett, J.W., and McMahon, S.B. (2002). Chondroitinase ABC promotes functional recovery after spinal cord injury. Nature *416*, 636–640.

Bregman, B.S., Kunkel-Bagden, E., Schnell, L., Dai, H.N., Gao, D., and Schwab, M.E. (1995). Recovery from spinal cord injury mediated by antibodies to neurite growth inhibitors. Nature *378*, 498–501.

Chen, M.S., Huber, A.B., van der Haar, M.E., Frank, M., Schnell, L., Spillmann, A.A., Christ, F., and Schwab, M.E. (2000). Nogo-A is a myelin-associated neurite growth inhibitor and an antigen for monoclonal antibody IN-1. Nature *403*, 434–439.

Cohen, N.R., Taylor, J.S., Scott, L.B., Guillery, R.W., Soriano, P., and Furley, A.J. (1998). Errors in corticospinal axon guidance in mice lacking the neural cell adhesion molecule L1. Curr. Biol. *8*, 26–33.

David, S., and Aguayo, A.J. (1981). Axonal elongation into peripheral nervous system "bridges" after central nervous system injury in adult rats. Science *214*, 931–933.

Davies, S.J.A., Goucher, D.R., Doller, C., and Silver, J. (1999). Robust regeneration of adult sensory axons in degenerating white matter of the adult rat spinal cord. J. Neurosci. *19*, 5810–5822.

Fawcett, J.W., and Asher, R.A. (1999). The glial scar and central nervous system repair. Brain Res. Bull. *49*, 377–391.

Fournier, A.E., and Strittmatter, S.M. (2001). Repulsive factors and axon regeneration in the CNS. Curr. Opin. Neurobiol. *11*, 89–94.

Fournier, A., GrandPré, T., and Strittmatter, S.M. (2001). Identification of a neuronal receptor mediating Nogo-66 inhibition of axonal regeneration. Nature *409*, 341–346.

Fruttiger, M., Montag, D., Schachner, M., and Martini, R. (1995). Crucial role for the myelin-associated glycoprotein in the maintenance of axon-myelin integrity. Eur. J. Neurosci. *7*, 511–515.

GrandPré, T., and Strittmatter, S.M. (2001). Nogo: a molecular deter-

minant of axonal growth and regeneration. Neuroscientist *7*, 377–386.

GrandPré, T., Nakamura, F., Vartanian, T., and Strittmatter, S.M. (2000). Identification of the Nogo inhibitor of axon regeneration as a Reticulon protein. Nature *403*, 439–444.

GrandPré, T., Li, S., and Strittmatter, S.M. (2002). Nogo Receptor antagonist peptide promotes axonal regeneration. Nature *407*, 547–551.

Hauben, E., Ibarra, A., Mizrahi, T., Barouch, R., Agranov, E., and Schwartz, M. (2001). Vaccination with a Nogo-A-derived peptide after incomplete spinal-cord injury promotes recovery via a T-cell-mediated neuroprotective response. Proc. Natl. Acad. Sci. USA *98*, 15173–15178.

Huber, A.B., Weinmann, O., Brösamle, C., Oertle, T., and Schwab, M.E. (2002). Patterns of Nogo mRNA and protein expression in the developing and adult rat and after CNS lesions. J. Neurosci. *22*, 3553–3567.

Kullander, K., Mather, N.K., Diella, F., Dottori, M., Boyd, A.W., and Klein, R. (2001). Kinase-dependent and kinase-independent functions of EphA4 receptors in major axon tract formation in vivo. Neuron *29*, 73–84.

Leighton, P.A., Mitchell, K.J., Goodrich, L.V., Lu, X., Pinson, K., Scherz, P., Skarnes, W.C., and Tessier-Lavigne, M. (2001). Defining brain wiring patterns and mechanisms through gene trapping in mice. Nature *410*, 174–179.

Li, C., Tropak, M.B., Gerlai, R., Clapoff, S., Abramow-Newerly, W., Trapp, B., Peterson, A., and Roder, J. (1994). Myelination in the absence of myelin-associated glycoprotein. Nature *369*, 747–750.

Liu, B.P., Fournier, A., GrandPré, T., and Strittmatter, S.M. (2002). Myelin-associated glycoprotein as a functional ligand for the Nogo-66 receptor. Science. *297*,1190–1193.

McKerracher, L., David, S., Jackson, D.L., Kottis, V., Dunn, R.J., and Braun, P.E. (1994). Identification of myelin-associated glycoprotein as a major myelin-derived inhibitor of neurite growth. Neuron *13*, 805–811.

Merkler, D., Metz, G.A., Raineteau, O., Dietz, V., Schwab, M.E., and Fouad, K. (2001). Locomotor recovery in spinal cord-injured rats treated with an antibody neutralizing the myelin-associated neurite growth inhibitor Nogo-A. J. Neurosci. *21*, 3665–3673.

Montag, D., Giese, K.P., Bartsch, U., Martini, R., Lang, Y., Bluthmann, H., Karthigasan, J., Kirschner, D.A., Wintergerst, E.S., Nave, K.A., et al. (1994). Mice deficient for the myelin-associated glycoprotein show subtle abnormalities in myelin. Neuron *13*, 229–246.

Mukhopadhyay, G., Doherty, P., Walsh, F.S., Crocker, P.R., and Filbin, M.T. (1994). A novel role for myelin-associated glycoprotein as an inhibitor of axonal regeneration. Neuron *13*, 757–767.

Neumann, S., and Woolf, C.W. (1999). Regneration of dorsal column fibers into and beyond the lesion site following adult spinal cord injury. Neuron *23*, 83–91.

Norton, W.T., and Poduslo, S.E. (1973). Myelination in rat brain: method of myelin isolation. J. Neurochem. *21*, 749–757.

Prinjha, R., Moore, S.E., Vinson, M., Blake, S., Morrow, R., Christie, G., Michalovich, D., Simmons, D.L., and Walsh, F.S. (2000). Inhibitor of neurite outgrowth in humans. Nature *403*, 383–384.

Ramón-Cueto, A., Cordero, M.I., Santos-Benito, F.F., and Avila, J. (2000). Functional recovery of paraplegic rats and motor axon regeneration in their spinal cords by olfactory ensheathing glia. Neuron *25*, 425–435.

Saruhashi, Y., Young, W., and Perkins, R. (1996). The recovery of 5-HT immunoreactivity in lumbosacral spinal cord and locomotor function after thoracic hemisection. Exp. Neurol. *139*, 203–213.

Savio, T., and Schwab, M.E. (1990). Lesioned corticospinal tract axons regenerate in myelin-free rat spinal cord. Proc. Natl. Acad. Sci. USA *87*, 4130–4133.

Schäfer, M., Fruttiger, M., Montag, D., Schachner, M., and Martini, R. (1996). Disruption of the gene for the myelin-associated glycoprotein improves axonal regrowth along myelin in C57BL/Wld^s mice. Neuron *16*, 1107–1113.

Simonen, M., Pedersen, V., Weinmann, O., Schnell, L., Buss, A., Ledermann, B., Christ, F., Sansig, G., van der Putten, H., and Schwab, M.E. (2003). Systemic deletion of the myelin-associated outgrowth inhibitor Nogo-A improves regenerative and plastic responses after spinal cord injury. Neuron *38*, this issue, 201–211.

Skene, J.H. (1989). Axonal growth-associated proteins. Annu. Rev. Neurosci. *12*, 127–156.

Wang, X., Chun, S.-J., Treloar, H., Vartanian, T., Greer, C.A., and Strittmatter, S.M. (2002a). Localization of Nogo-A and Nogo-66 Receptor proteins at sites of axon-myelin and synaptic contact. J. Neurosci. *22*, 5505–5515.

Wang, K.C., Koprivica, V., Kim, J.A., Sivasankaran, R., Guo, Y., Neve, R.L., and He, Z. (2002b). Oligodendrocyte-myelin glycoprotein is a Nogo receptor ligand that inhibits neurite outgrowth. Nature *417*, 941–944.

Yokoyama, N., Romero, M.I., Cowan, C.A., Galvan, P., Helmbacher, F., Charnay, P., Parada, L.F., and Henkemeyer, M. (2001). Forward signaling mediated by ephrin-B3 prevents contralateral corticospinal axons from recrossing the spinal cord midline. Neuron *29*, 85–97.

Zambrowicz, B.P., Friedrich, G.A., Buxton, E.C., Lilleberg, S.L., Person, C., and Sands, A.T. (1998). Disruption and sequence identification of 2,000 genes in mouse embryonic stem cells. Nature *392*, 608–611.

Zheng, B., Ho, C., Li, S., Keirstead, H., Steward, O., and Tessier-Lavigne, M. (2003). Lack of enhanced spinal regeneration in Nogo-deficient mice. Neuron *38*, this issue, 213–224.